Chapter 3 Microstructure and Mechanical Properties of Additively Manufactured Ti-6Al-4V Alloy

In this chapter, the effect of build orientation and heat treatment on density, residual stress, microstructure, and microhardness are discussed in detail. This chapter describes the findings of EBSD and SEM analysis. This chapter also includes the tensile test results and fractography of the tested samples.

3.1 Results and discussion

3.1.1 Characterization of powder

The distribution of powder particle size of the alloy Ti-6Al-4V is shown in the form of histograms in Figure 2.1(c); the size ranges from 4 to 40 μm. SEM micrographs in Figure 2.1 (a and b) show spherical morphology of powder particles. During the process of gas atomization, flowing molten metal gets fragmented into droplets due to stream of gas, resulting in powder particles of nearly spherical shape. Sieving can be used to separate powder particles of desired size for L-PBF [175]. In general, the range of powder particle size should be 10 - 45 μm. In this study, the average size of powder has been taken as 20 μm for fabrication by L-PBF process.

3.1.2 Density

Archimedes' principle has been used to measure the density of the fabricated components as it is simple and economical. Archimedes' test outcomes are calculated by weighing the component in dry condition as well as submerged-in-water and the results are displayed in Table 3.1. The theoretical density of Ti-6Al-4V is 4.41 g/cm^3. Densities of 0° and 45° samples are more than 99% of the corresponding theoretical density. The density of 90°

oriented components is less as compared to 0° and 45° build-oriented components due to presence of defects like pores, un-melted powder, etc. Figure 3.1 shows SEM micrographs of the pores in the AB components, consisting of macropore and small pores in the surrounding and the shape of the pore is almost spherical.

Table 3.1 Density and surface roughness of AB samples fabricated with three build orientations

Build orientation	**Density (g/cm^3)**	**Surface roughness (µm)**		
		R_a	R_z	R_q
0°	4.403	3.57	17.3	4.39
45°	4.401	5.94	28.0	7.18
90°	4.336	4.16	21.6	5.09

L-PBF process is a process of layered style melting and solidification in which the orientation of components from the build plate influences the density of AB-condition components as shown in Table 3. An overhang, a 45° build-oriented component is formed with supporting structure in some portions as shown in Figure 2.2 (c). The direction of heat dissipation during solidification would be opposite to the build direction; due to this crystal structures are parallel to the direction of build. Powder particles have a significantly lower thermal conductivity with respect to solid counterpart [176]. When the next layer is deposited, some portions of solid component and some portions of the powder particles are available underneath this layer in the heat dissipation direction (Figure 3.12).

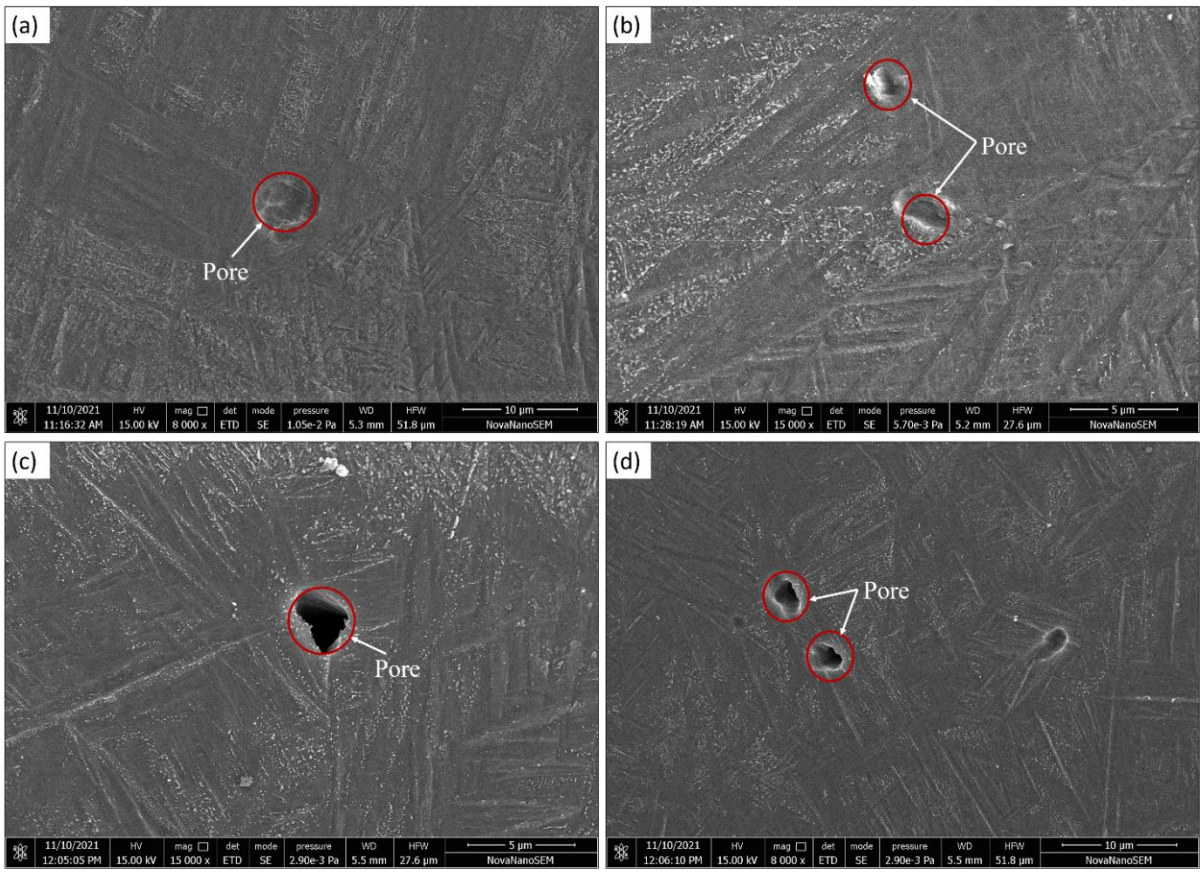

Figure 3.1 Pores identified in the as-built (a, b) 45° and (c, d) 90° build-orientation samples (X8000 and X15000)

For 45° build-oriented components, more amount of powder particles will be present, due to this, the thermal conductivity decreases. As thermal conductivity decreases, the temperature of the molten pool increases and deeper penetration of the molten pool occurs [177]. For the same energy supplied, a deeper molten pool is obtained in case of a high concentration of energy due to the presence of more powder particles [15], that could not transmit heat from the component because of less thermal conductivity, and that caused more energy accumulation in the molten pool. Excess accumulation of energy increases the molten pool's penetration depth. As a consequence, it may form bubbles and cause oscillation [178]. Bubbles, being in a gaseous state, can freely move around in the molten pool. During fabrication, the rate of solidification is very fast in the L-PBF

process; hence, these gas bubbles could not get sufficient time to escape away from the surface and formed defects like pores, as also mentioned by Khorasani et al. [32]. The more powder in the heat dissipation direction for the 45° build-oriented component produces more pores, this is consistent with the measured results. Fabrication of the components in 90° orientation requires a greater number of layers than those of other oriented components, and that results in an increase in number of pores. Due to that the density of 90° oriented components is the lowest among the three build-oriented components.

3.1.3 Surface roughness

Surface roughness of the heat-treated components fabricated in the three different build orientations by L-PBF process was determined and is presented in Table 3.1. Surface roughness of the 45º oriented component is the highest among the three build orientations because of the higher accumulation of energy [11]. For the 45° build-oriented component, due to larger quantity of powder particles and consequent decrease in thermal conductivity, accumulation of energy increased during melting. It caused partial melting of surrounding powder particles due to which surface roughness of the component increased. In this study, the average surface roughness values varied from 3 to 6 μm and it is comparable to the result reported by Mower and Long [179].

3.1.4 Microhardness

Microhardness of the AB and HT samples for the three build orientations have been shown in Figure 3.2. The highest microhardness was found in the AB sample in 0° orientation (481.25 $HV_{0.2}$) and was lowest in the HT sample built in 0° orientation. For the AB condition, the microhardness are 481.25 $HV_{0.2}$, 470.53 $HV_{0.2}$, and 479.75 $HV_{0.2}$ for the 0°, 45°, and 90° orientations, respectively and after HT, the microhardness are

427.81 $HV_{0.2}$, 469.10 $HV_{0.2}$, and 441.17 $HV_{0.2}$ for the 0°, 45°, and 90° orientations, respectively. The average microhardness for the AB and HT conditions was measured as 477.17 $HV_{0.2}$ and 446.03 $HV_{0.2}$, respectively.

For the AB condition, higher hardness has been observed due to the high cooling rate and the formation of very fine α′ martensitic laths, as shown in Figure 3.2. The average hardness of the different build orientations shows a consistent trend of being the highest for the 0° orientation and lowest for the 45° orientation, as also mentioned by Thijs et al. [12]. The hardness of 90º and 45º oriented components is lower due to the presence of voids, un-melted powders, and cracks. The variation in hardness has been observed due to various defects noticed on the surface of the components.

Variation in hardness after the HT is directly in relation to the change in the phase of the as-built component. By heat treating at 800 ºC for 1.5 h in argon atmosphere and furnace cooling, the stresses associated with the as-built components have been relieved, as mentioned in the Table 3.2, and could be influencing the hardness after the heat treatment, as reported by Wu et al. [180]. Due to heat treatment, the martensitic α′ phase fully transformed into α and β phases and fractional volume of the soft β phase increased with respect to the α phase. This is main reason for the reduction in hardness of the HT components [70].

There is no significant change in hardness of the 45º oriented component before and after HT. The hardness of the 45º oriented component in HT condition shows a significantly higher value than the other two build-oriented components. According to EBSD and XRD analysis, the β fraction peak intensity shown in Figure 3.4 is not changing significantly for the 45° oriented component after the heat treatment. It is well known that when the β fraction is increased, the components exhibit increased ductility

and reduced hardness, which can be seen in the 0° and 90° oriented components (Figure 3.2). After heat treatment, the peak position in grain size distribution of the 45° oriented component is still in the fine grain region and has not changed significantly (Figure 3.9), which also explains why the hardness has not changed. Presence of low residual stresses provides lesser driving energy for transformation during heat treatment of inclined components.

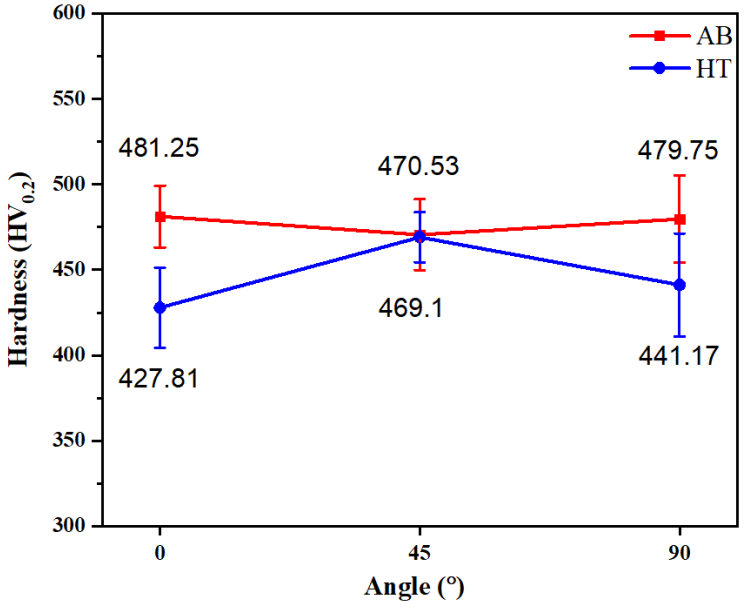

Figure 3.2 Hardness of the AB and HT samples in different orientations

3.1.5 Residual stress

Due to high cooling rate and layer by layer deposition during the L-PBF fabrication, it was found that considerable tensile residual stresses have been induced in the AB components. The tensile residual stress can be completely eliminated by exposure at 800 °C for 1.5 h, as reported by Wauthle et al. [65]. In this investigation, the value of residual stress is proportional to the number of layers (component height) for the different build orientations and the results are shown in Table 3.2. After HT, the residual stress is almost

negligible (Table 3.2). Ahmad et al. [55] mentioned that residual stress is generated due to many factors such as component height, heat transfer conditions, complexity of components, and support structure [181].

Table 3.2 Tensile residual stress along the length of the tensile samples of L-PBF components in AB and HT conditions in the three build orientations

Component	Tensile residual stress (MPa)
AB-0°	77.9 ± 2.85
AB-45°	70.4 ± 4.81
AB-90°	163.1 ± 7.26
HT-0°	5.8 ± 0.56
HT-45°	2.6 ± 0.55
HT-90°	1.6 ± 1.27

The heat-affected region around the molten pool experiences high thermal stresses when metal powder melts due to the laser beam. The melt zone hardens and diminishes when the source of heat is withdrawn from the molten zone. Shrinkage is more in the molten pool in comparison with that in the adjoining heat-affected region because of the higher temperature of the molten pool with respect to the heat-affected zone. However, the shrinkage phenomenon gets hampered by the nearby heat-affected zone, as a result, tensile stress is induced in the nearby solidified region.

The residual stress is influenced by the difference in temperature between the new solidified layer and the previously solidified layer. For the same energy input, the difference in temperature depends on the degree of inclination; large inclination of components results in low residual stress because of more powder, as thermal conductivity of powder particles is very less in comparison with that of the corresponding solid component in the supporting area that lowers heat dissipation.

For the 45º oriented component, in the supporting area, more powder particles come below the new solidified area. Therefore, for the same energy input, the temperature difference between the new solidified layer and the previous layer reduces, and that

lowers the heat dissipation. As a result, the residual stress reduces in the 45º oriented component. However, in the case of 0º and 90º oriented components, during deposition of the new layer, the previous layer is also metallic and the thermal conductivity of metal is very high as compared to metal powder and less quantity of powders lies below the new solidified layer. As a consequence, high heat dissipation through the already formed metallic layer increases the thermal gradient between the new solidified layer and the previous layer, and the residual stress increases. Thus, the maximum residual stress is generated in the 90º oriented component as compared to the 0° and 45º oriented components as shown in Table 4.

The residual stress is also influenced by the component height and defects like pores and cracks. In 90º oriented component, the number of layers is large as compared to the other build-oriented components, it increases the residual stress in the component, and also, increases the number of pores as shown in Figure 3.1, as also observed by Ren et al. [15]. The order of residual stress is $\boldsymbol{Residual\ stress_{90^\circ} > Residual\ stress_{0^\circ} > Residual\ stress_{45^\circ}}$. After heat treatment, the value of tensile residual stress drastically reduced and became negligible (Table 3.2).

3.1.6 Microstructure of as-built and heat-treated L-PBF Ti-6Al-4V alloy

During L-PBF process, because of the high cooling rate of $10^4 - 10^5$ K/s [182], the as-built microstructure consisted of fine acicular α′ martensite phase inside prior-β grains and is almost oriented along the direction of build as it solidifies in the direction of heat dissipation [183]. During the process, the molten metal solidifies with the same crystal direction because it grows epitaxially. It involves incomplete re-melting of the preceding solidified layer and acts as a nucleus for epitaxial growth. In this study, the influence of

build orientations on the microstructure of as-built L-PBF Ti-6Al-4V fabricated at 0°, 45°, and 90° has been investigated. The important microstructural features like pores, prior-β grains, and crystallography textures have also been studied as they have a considerable impact on tensile properties and crack formation in theTi-6Al-4V alloy [184].

Figure 3.3 (a_1, b_1, and c_1) and (a_2, b_2, and c_2) show the microstructures of the AB and the HT samples at three different orientations of 0°, 45°, and 90° respectively. The pore defects are randomly distributed in the microstructure (Figure 3.3 a_1 and Figure 3.1). In the current study, it was noticed that the defects in L-PBF of α+β titanium alloys can be initiated due to non-uniform powder bed distribution, as reported by Yan et al. [69]. The prior-β grains have irregular polygons and a grain size of 100-150 μm (Figure 3.3). On the other hand, the columnar grains typically grow up to many layers of deposition and reach a height of several hundreds of micrometers as shown in Figure 3.3 (a_1, b_1, and c_1). Due to the high content of Vanadium in the α′ martensite phase, this phase is in supersaturated condition but exhibits the same crystal structure as the α phase.

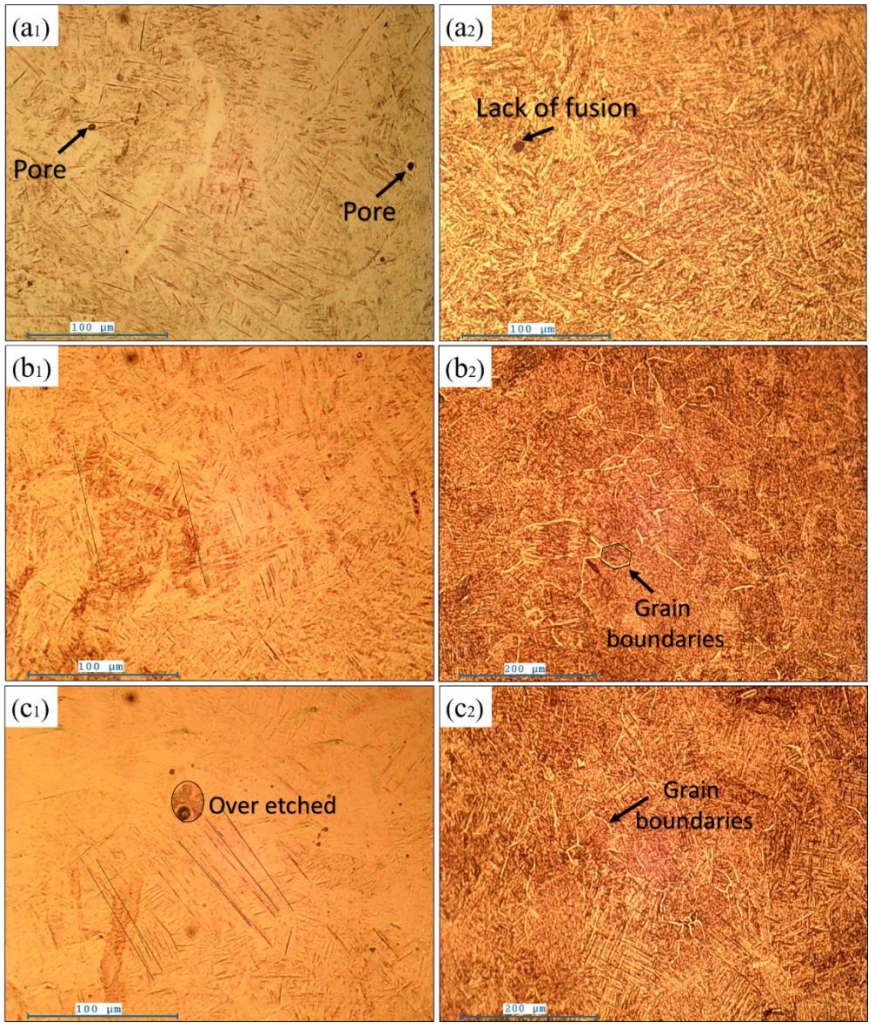

Figure 3.3 Optical micrographs of the longitudinal sections of the samples in different conditions with different orientations: (a) 0°, (b) 45°, and (c) 90°; subscripts 1 and 2 represent the as-built and heat-treated conditions respectively

The XRD analysis result is illustrated in Figure 3.4 (a and b) to reveal the phases present over the entire portion of the components. In the AB condition there is a hexagonal close-packed (HCP) structure, as per the XRD analysis (Figure 3.4 a). Based on the acicular morphology and crystal structure of the phase, as well as previous findings, the HCP phase in the AB condition is assumed to represent the α′ martensitic phase [184]. The XRD patterns of the AB condition (Figure 3.4 a) do not show peak of the β phase. However, a tiny peak of the β (110) phase is noticed between the α (002) peak and the α

(101) peak after heat treatment (inset of Figure 3.4 b) because of less volume fraction of the β phase. Therefore, for the HT samples, the constituent phases are α and β.

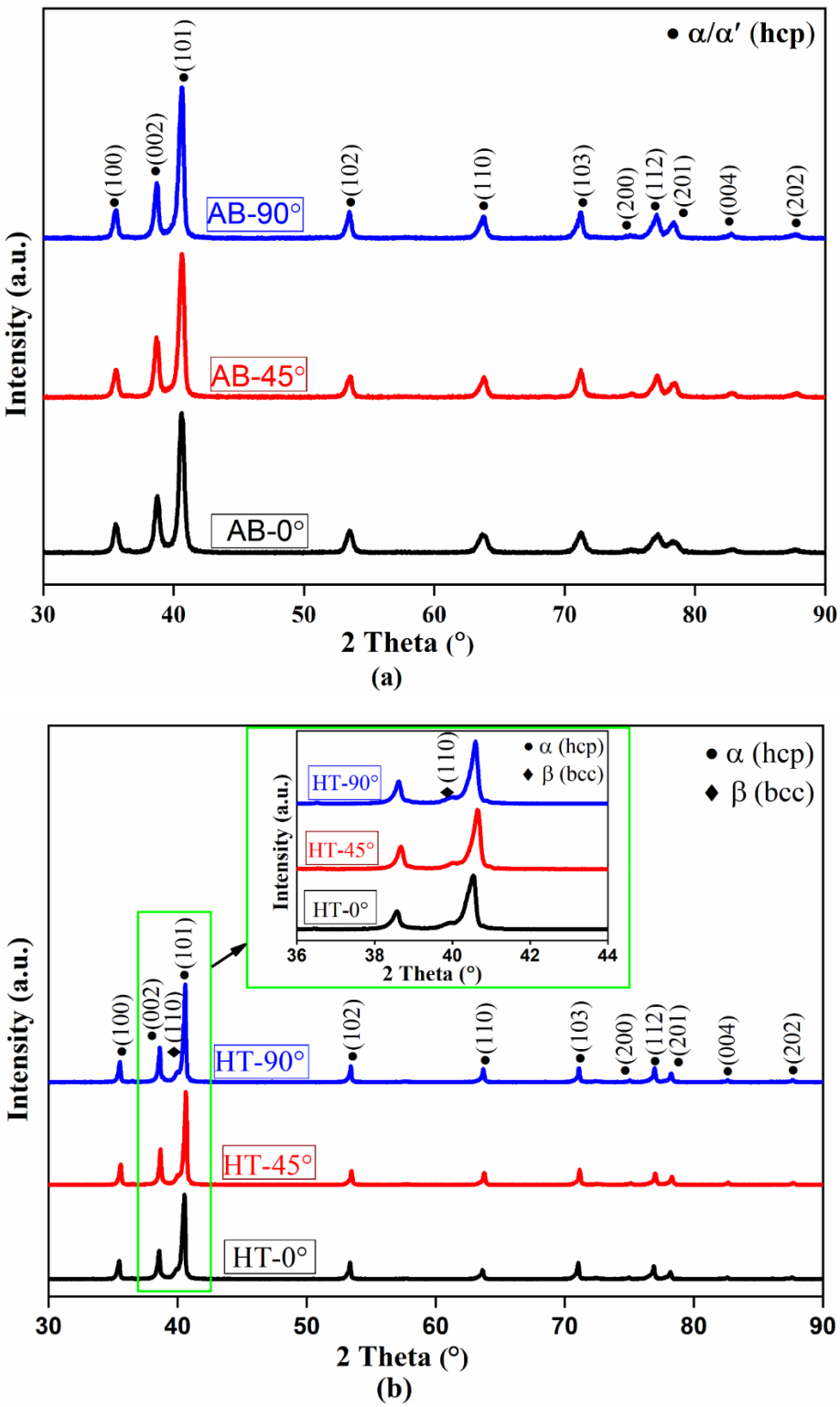

Figure 3.4 X-ray diffraction (XRD) analysis of longitudinal sections of the samples in different conditions with different orientations: (a) as-built and (b) heat-treated. The inset in (b) is the local XRD pattern of the HT samples

Figure 3.5 shows SEM micrographs of the AB and HT samples of different orientations. The microstructure of the AB samples is totally martensitic α′ at room temperature. According to SEM micrographs, the microstructure of AB and HT types are relatively distinct, but there is no notable difference in the microstructure at different build orientations for the same type. As shown in Figure 3.5 (a_1, b_1, and c_1) for the AB condition, long and columnar grains are aligned roughly along the direction of the build. These grains are recognized as prior-β grains [178], having a width of ~120 μm, equivalent to hatch distance and a length up to several millimetres. The fine acicular structure is surrounded by columnar grains, roughly 10 to 140 μm long and approximately 1 μm wide.

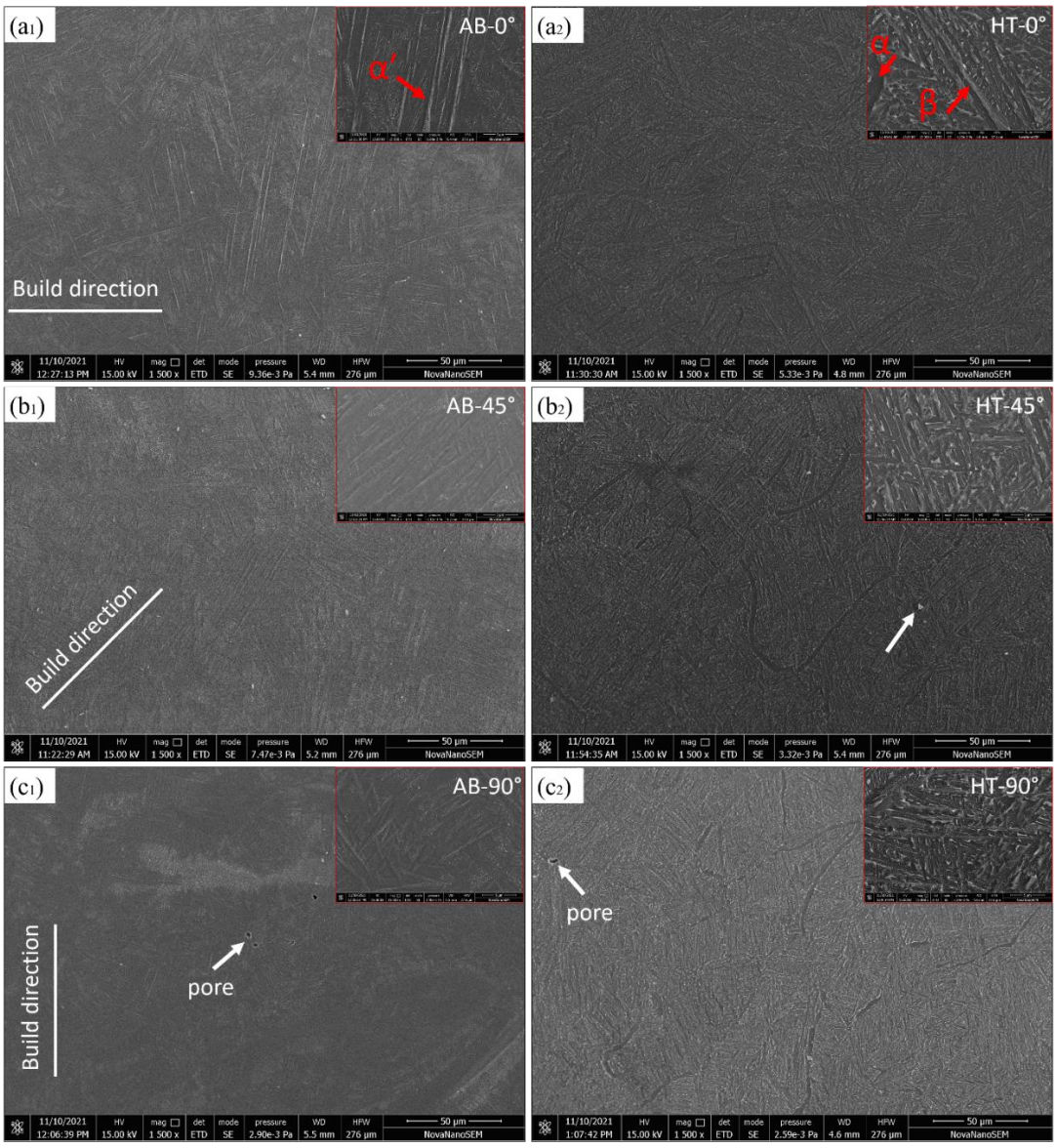

Figure 3.5 Scanning electron micrograph of the longitudinal section of samples in different conditions with different orientations: (a) 0°, (b) 45°, and (c) 90°; subscripts 1 and 2 represent the as-built and heat treatment conditions respectively

The optical and SEM micrographs also revealed that the AB components are influenced by columnar grains, which are filled with very fine α′ martensite laths. The columnar grain boundaries constitute the prior-β grains produced during cooling [185]. Because the Ti-6Al-4V alloy fabricated by L-PBF experiences an exceptionally high cooling rate [8], the β phase of Ti-6Al-4V alloy is completely transformed into fine α′ martensitic phase.

According to the requirements for aerospace [3] and implant materials, it is preferred to have a homogeneous and stable microstructure of L-PBF components [186]. However, the as-built Ti-6Al-4V components show unstable behaviour, with very fine highly textured microstructure, and the presence of residual stress due to high thermal gradient, influenced by the exceptionally fast-moving laser beam during fabrication, which may induce some defects like cracks, and pores, which reduce ductility and are not considered for desired applications [8]. Therefore, for a completely stable and homogeneous microstructure, the heat treatment process is of considerable interest.

After the heat treatment of L-PBF Ti-6Al-4V at 800 °C for 1.5 h [10], the β phase nucleates along the α′ grain boundaries as shown in the SEM microstructure (inset of Figure 3.5 (a_2)). The α′ phase has supersaturated vanadium (V) and after heat treatment, the V atoms come out from the α′ phase, as a result of which V is locally enriched and β phase forms along the grain boundaries. As the V atoms migrate from α′ to β, there is a reduction of free energy of α′ supersaturated solid solution, and consequently, α′ phase is progressively converted into the α phase. The temperature during the HT was high enough to convert the α′ martensitic phase but could not affect the grain orientation. It is clear from the analysis of electron backscatter diffraction as shown in Figure 3.7. It is also in agreement with the results of the XRD analysis (Figure 3.4 b) which reveals the presence of α as well as β phase [110] plane in the HT type.

Various types of defects are also observed after the fabrication of Ti-6Al-4V by the L-PBF process, as seen in Figure 3.3 and Figure 3.5. One of the most common defects is pores, present in the AB condition, which affect the density of the components. One of the main causes of porosity defects is the formation of gas during manufacturing due to high laser beam intensity, gases dissolve in the molten pool and are entrapped during

solidification because of the high cooling rate. To resolve this issue, the size of the molten pool is reduced by reducing the laser power or layer thickness [187]. Another observed defect is a lack of fusion due to an inhomogeneous powder bed, as mentioned by Ren et al. [15]. This defect can be resolved by reducing the thickness of the layer to melt properly the previously solidified layer of materials and enhancing the bonding of the already solidified layer with a new solidified layer.

Figure 3.6 (a) and (b) show the results of an EDS analysis of the L-PBF fabricated Ti-6Al-4V components for elemental distribution in different phases present in AB and HT types, respectively. In AB type, three spots were examined and the average weight percentages of Ti, Al, and V was found 87.74, 6.62, and 5.65, respectively, which is closer to chemical composition of the Ti-6Al-4V powder particles.

After heat treatment of L-PBF Ti-6Al-4V at 800 °C for 1.5 h, the β phase nucleated along the α′ grain boundaries. The α′ phase had supersaturated vanadium (V). During heat treatment, V atoms come out from the α′ phase; as a result of which V is locally enriched and β phase forms along the grain boundaries (Figure 3.6 b). To confirm this hypothesis, EDS analysis was performed on heat-treated components, where white β phase and dark α phase were present. Four spots (two spots of the white β phase and two spots of the dark α phase) were examined. The average weight percentages of Ti, Al, and V were 82.11, 6.54, and 11.35 in white β phase, and 88.63, 7.51, and 3.87 in dark α phase, respectively. As the V atoms migrated from α′ to β, there was a reduction of free energy of α′ supersaturated solid solution. Thus, α′ phase was progressively converted into α phase.

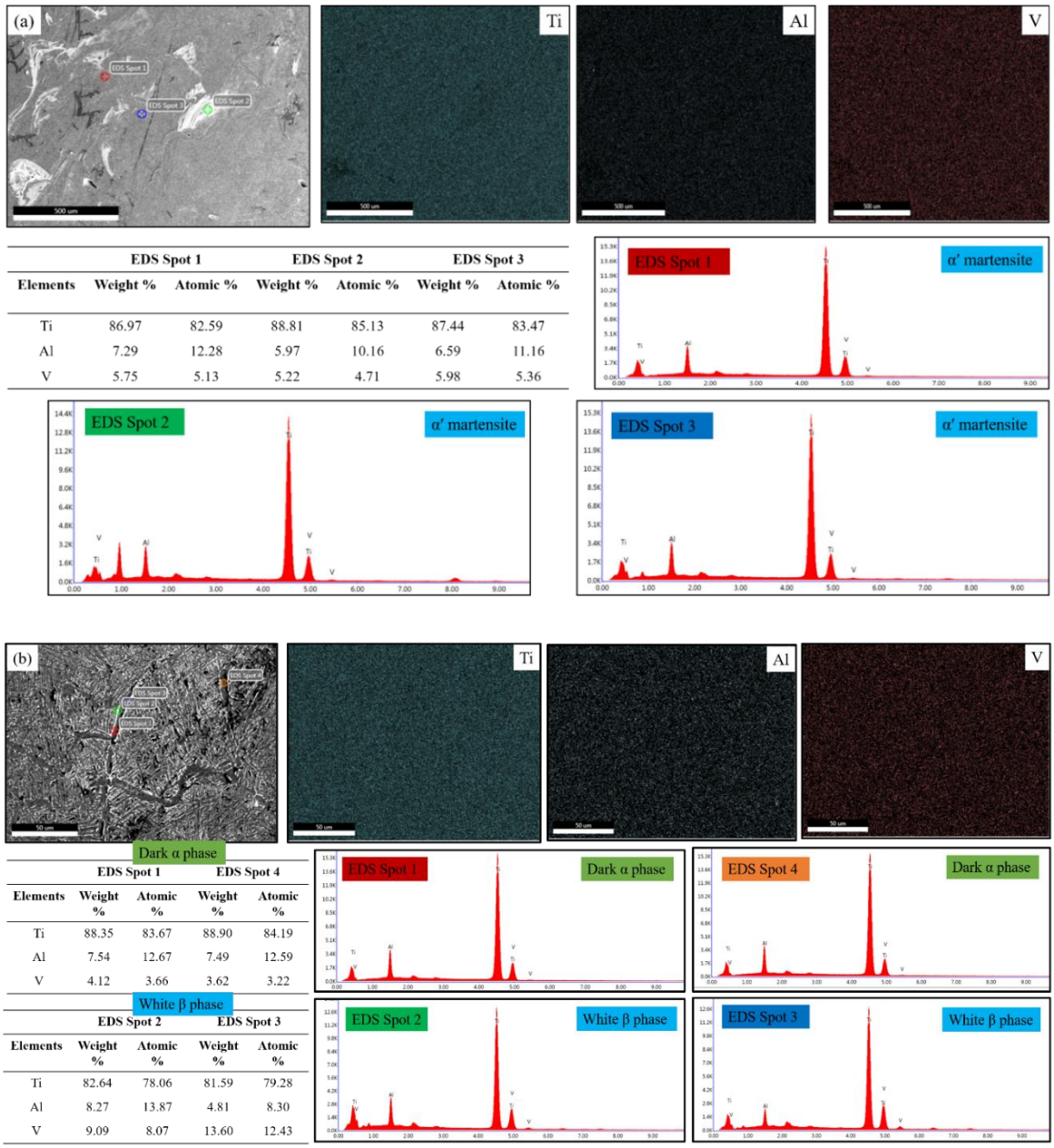

	EDS Spot 1		EDS Spot 2		EDS Spot 3	
Elements	Weight %	Atomic %	Weight %	Atomic %	Weight %	Atomic %
Ti	86.97	82.59	88.81	85.13	87.44	83.47
Al	7.29	12.28	5.97	10.16	6.59	11.16
V	5.75	5.13	5.22	4.71	5.98	5.36

	EDS Spot 1		EDS Spot 4	
Elements	Weight %	Atomic %	Weight %	Atomic %
Ti	88.35	83.67	88.90	84.19
Al	7.54	12.67	7.49	12.59
V	4.12	3.66	3.62	3.22

	EDS Spot 2		EDS Spot 3	
Elements	Weight %	Atomic %	Weight %	Atomic %
Ti	82.64	78.06	81.59	79.28
Al	8.27	13.87	4.81	8.30
V	9.09	8.07	13.60	12.43

Figure 3.6 Scanning electron micrographs and energy-dispersive spectrum (EDS) analysis of the L-PBF Ti-6Al-4V components in (a) AB and (b) HT conditions

3.1.7 Texture

Figure 3.7 shows micro-texture of the inverse pole figure orientation map and their corresponding (0001) pole figures of components in AB and HT types with different build orientations. Figure 3.7 (a_1), (b_1), and (c_1) correspond to AB condition and Figure 3.7 (a_2),

(b_2), and (c_2) for HT condition for the 0°, 45° and 90° orientations, respectively. From the figures, it can be noticed that preferred crystal directions are present in AB components and are also dependent on the build direction. Texture has also been found in the HT condition.

The pole intensity value acquired from (0001) pole figures are shown in Figure 3.8 (a) to check the texture intensity of the components. The value of pole intensity obtained in the 0º and 45º component shows a similar trend for the AB and HT type. However, the value of pole intensity in the 90º component was exceptionally high as shown in Figure 3.8 (a). The number fractions of the misorientation angle of AB and HT types are shown in Figure 3.8 (b). The area fraction of grain diameter for different build orientations in AB and HT types is shown in Figure 3.8. The diameter of the grains increases after the heat treatment but there is not much dependency on the build orientation.

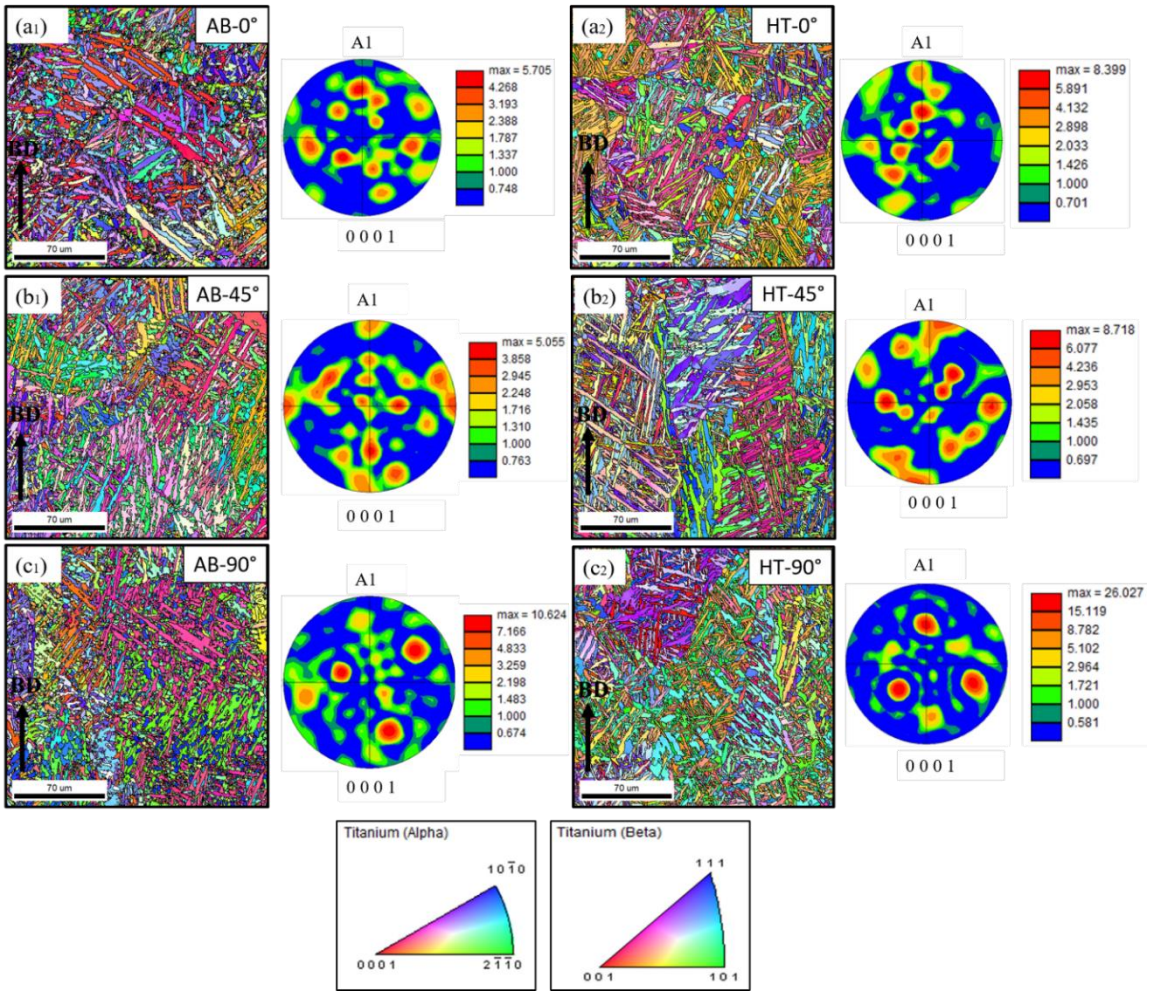

Figure 3.7 The inverse pole figure orientation maps and their corresponding (0001) contour pole figures of the longitudinal section of samples in different conditions with different orientations obtained by electron backscatter diffraction: (a) 0°, (b) 45°, and (c) 90°; subscripts 1 and 2 represent the as-built and heat treatment conditions, respectively

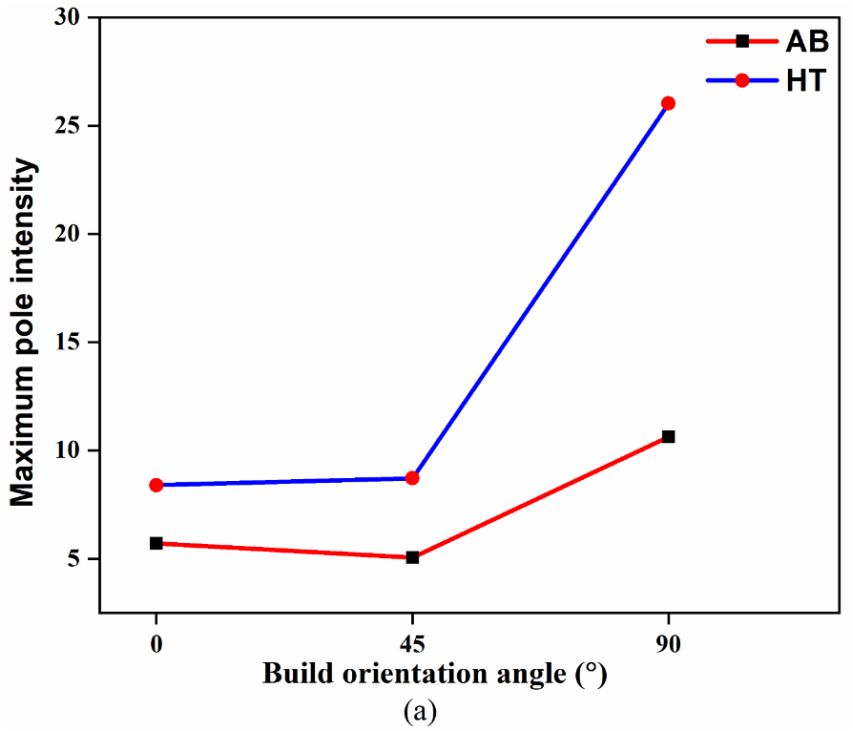

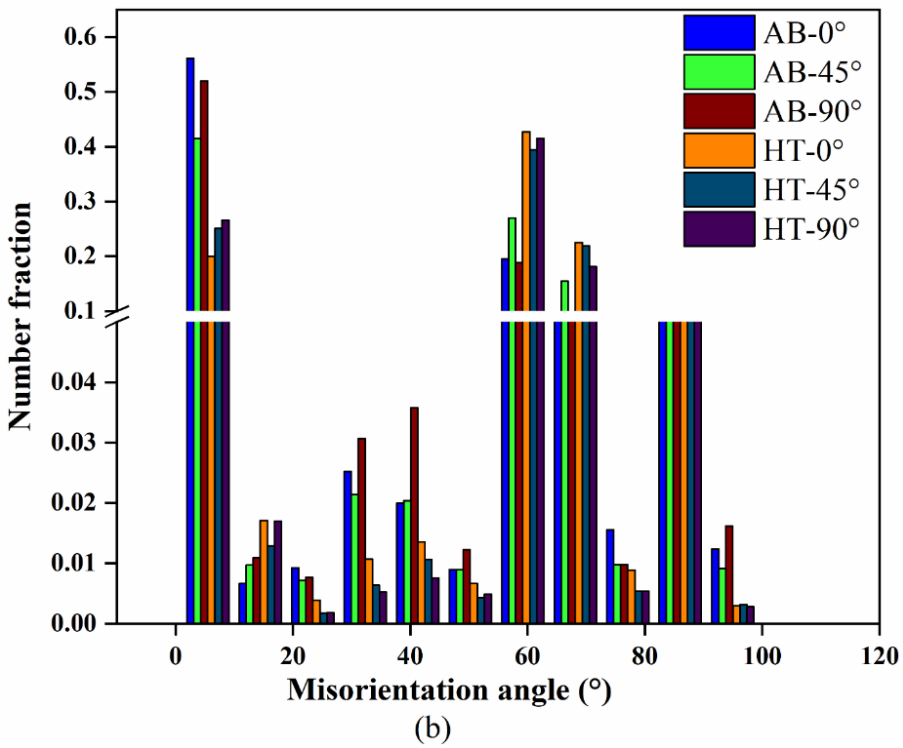

Figure 3.8 Texture analysis: (a) The maximum pole intensity and (b) misorientation angles in different conditions and different build orientations

During the solidification process, the fine α′ martensitic phase and prior β grains are interlinked by the phase transformation in the AB condition. During HT, α′ martensite transforms into α and β phases. This mutual transformation of phases creates a texture transformation between both the phases. Hence, the formation of fine acicular α′ martensitic grains is observed in Figure 3.7 (a_1, b_1, and c_1). The orientation angle (OA) below 15º is defined as the low angle grain boundary, whereas OA above 15º is defined as the high angle grain boundary [188].

An area fraction versus grain size distribution is shown in Figure 3.9. The average grain size diameter increases after the heat treatment. The highest area fraction of the grain size ranging from 3 to 5 µm has been observed as compared to the other grains distributed non-uniformly throughout the microstructure in the as-built conditions as shown in Figure 3.9 (a, b, and c). This indicates the formation of finer grains during fabrication by L-PBF process, which can also be confirmed by the number fraction versus misorientation angle graph displayed in Figure 3.8 (b). The movement of dislocations through a material is disrupted by grain boundaries; hence, lowering grain size is a typical approach to improve tensile strength.

After heat treatment, the highest area fraction of grain size ranges from 5–7 µm as shown in Figure 3.9 (d, e, and f). The number fraction versus misorientation angle graph is displayed in Figure 3.8 (b). The highest number fraction of low angle grain boundary has been observed in AB condition with some fraction of the high angle grain boundary (Figure 3.8 b), which clearly indicates the presence of fine α′ phase. However, the highest number fraction of high angle grain boundaries has been seen with less number fraction of low angle grain boundaries in the HT type [189].

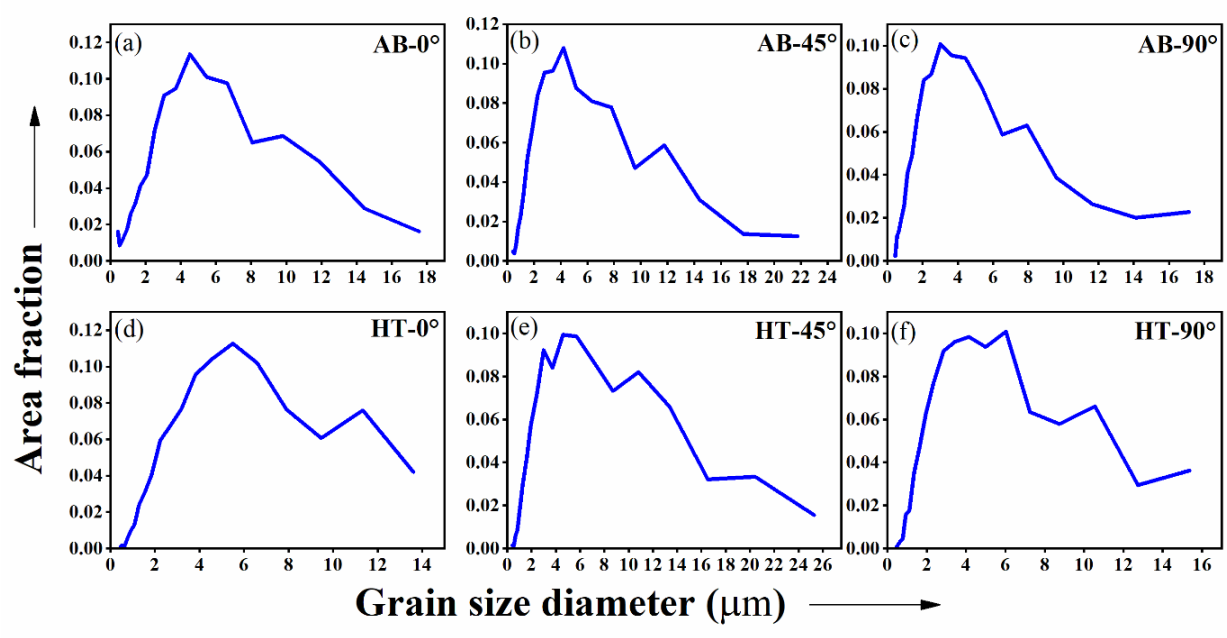

Figure 3.9 Grain size distribution in different conditions with different build orientations: (a) AB-0º, (b) AB-45º, (c) AB-90º, (d) HT-0º, (e) HT-45º, and (f) HT-90º

3.1.8 Strength properties of as-built and heat-treated L-PBF Ti-6Al-4V specimens

Two AB and two HT tensile samples were tested and all the specimens failed in the gauge section after a significant amount of elongation. The tensile stress-strain curves are shown in Figure 3.10. Figure 3.11 shows the variation of the UTS, yield strength, and percentage elongation at fracture. As shown in Figure 3.10 and Figure 3.11, in AB type, the mechanical properties vary significantly with respect to build orientation. For AB type, the UTS decreases with increase of build orientation from 0º to 90º. The values of YS and UTS reach the maximum of 1093.45 MPa, and 1202.29 MPa, respectively for 0º. The YS is the minimum (1046.51 MPa) at 45º build orientation. The UTS is the minimum (1094.16 MPa) at 90º build orientation. The elongation at fracture also changes with the build orientation, the maximum of 8.04 % at 90º and the minimum of 7.64 % at 0º.

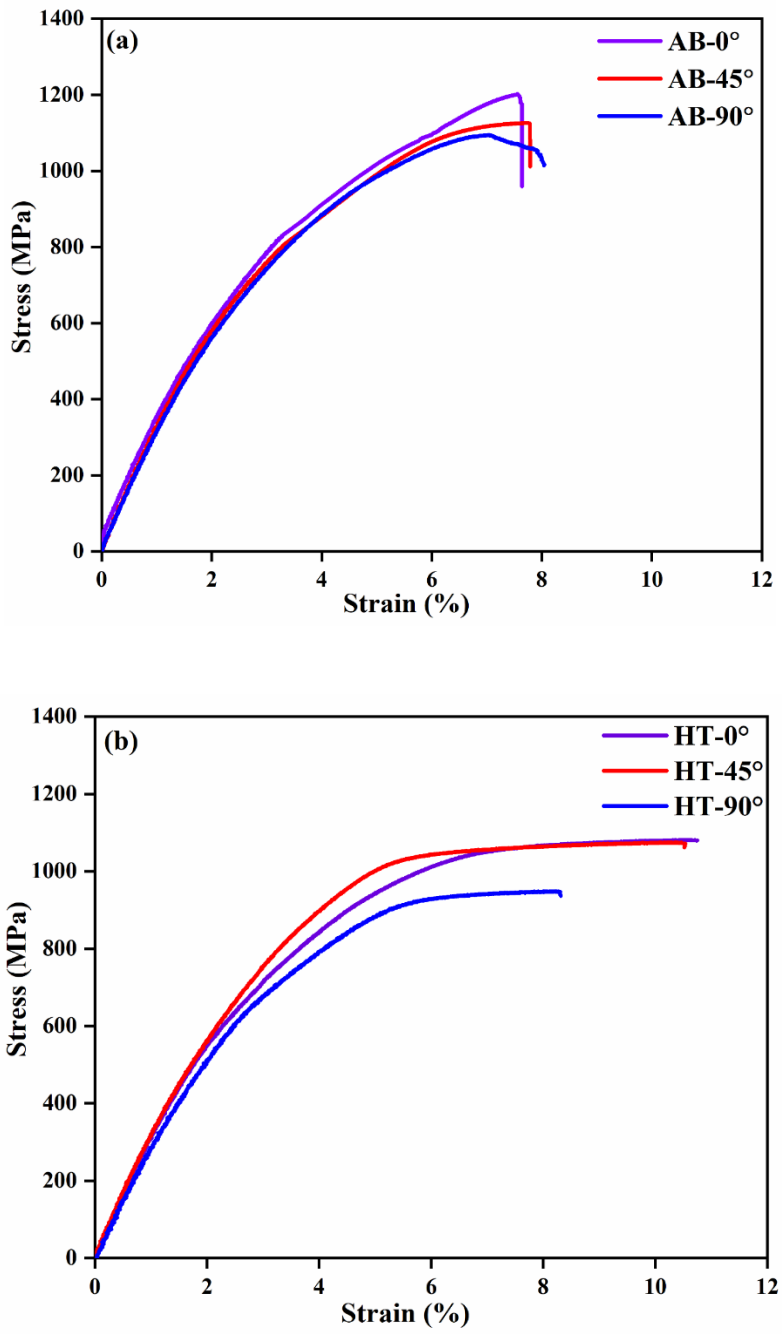

Figure 3.10 Tensile stress-strain curve of the longitudinal section of specimens in different conditions with different orientations: (a) AB condition and (b) HT condition

For the HT type also, the changes in mechanical properties are noticeable with respect to build orientation. The heat treatment reduces YS and UTS of samples, reaching the maximum values of 1024.15 MPa, and 1081.22 MPa, respectively, at 0º, and the minimum values of 906.56 MPa, and 948.41 MPa, respectively at 90°. In contrast with

the AB type, for the HT type, the elongation at fracture increases, reaching the maximum of 10.79 % at 0º, and the minimum of 8.29 % at 90º.

The UTS and YS of AB samples are higher in comparison with that of the HT specimens due to the formation of fine grains of α, α′ martensitic phase (Figure 3.7) after fabrication by the L-PBF process. After HT, the martensitic α′ phase transforms to α+β phases, hence the strength of specimens is reduced. Also, the elongation at fracture increases after HT as compared to AB specimens. The major disadvantage of L-PBF Ti-6Al-4V alloy is poor elongation in AB conditions and this is the reason for HT to enhance ductility of the specimens. The AB component consisted of α′ martensite phase, which does not create colonies of laths (Figure 3.7), due to which it shows poor elongation at fracture [185]. On the other hand, in the HT specimens, some β phase retained at the α laths' grain boundaries, contributes to improve the ductility due to slip transfer at the interface of α/β phase [190].

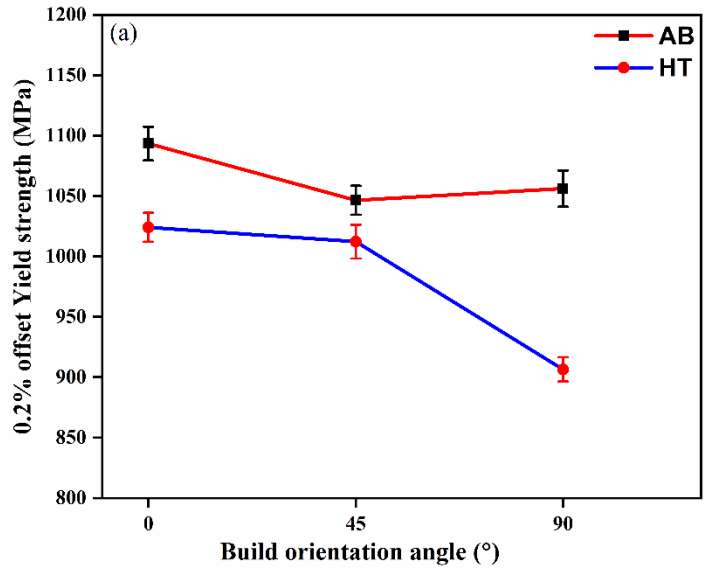

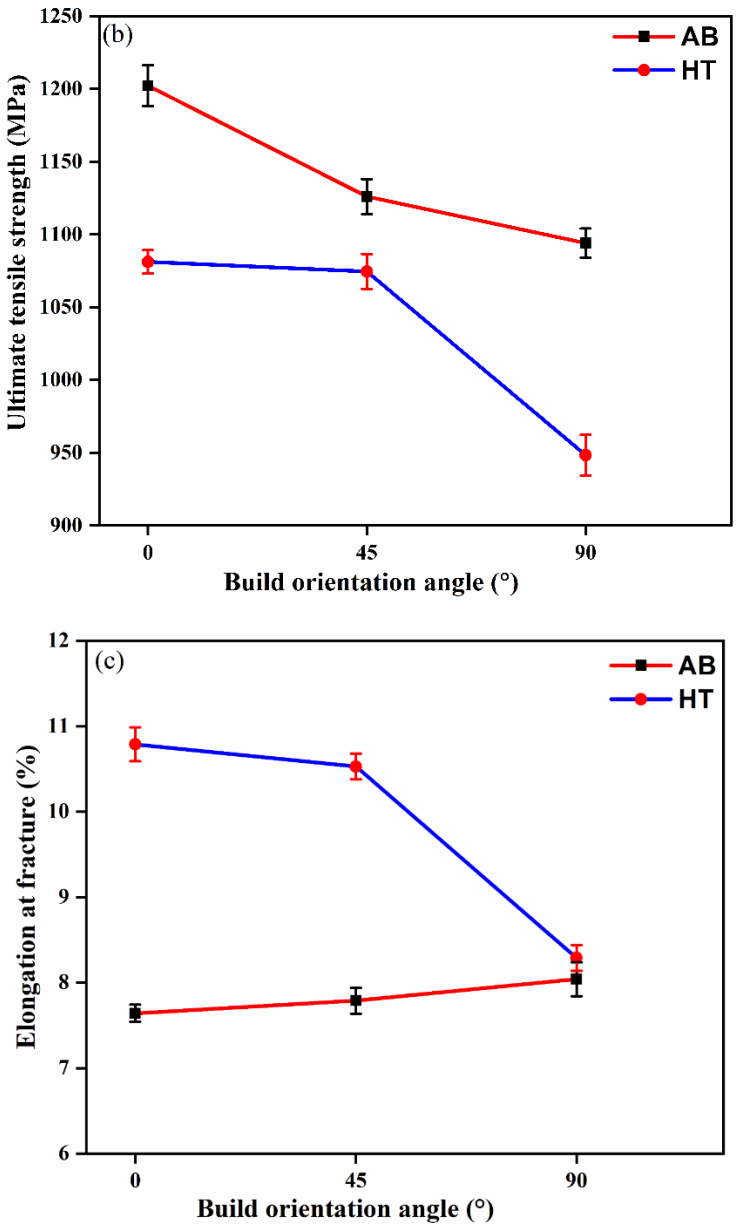

Figure 3.11 Tensile properties of AB and HT specimens with different build orientations: (a) yield strength, (b) ultimate tensile strength, and (c) elongation at fracture

The tensile properties of the flat, inclined, and upright orientations were studied in the same condition and significant differences were noticed in the components under three orientations in the AB condition. However, very less difference is observed in the HT specimens. As discussed in the Introduction section, residual stress, pores, and texture are the main contributors for the difference in behavior under tensile loading. The tensile residual stresses generated during the L-PBF process affect the tensile properties of AB

components significantly. The heat treatment mitigates the effect of tensile residual stresses.

The value of residual stress is influenced by component height and defects like pores and cracks. A 90° oriented component has large number of layers (1700) as compared to other build-oriented components, increasing the residual stress in the component. The higher tensile residual stress present in 90º build oriented components (Table 3.2) created more defects. When a load is applied to the sample and exceeds the critical value of crack initiation, this may lead to separation of the layers. The AB 90° oriented components have the largest tensile residual stress, due to which most potential cracks were developed. When the axis of load applied is parallel to the deposition direction, it is more favorable for creation and propagation of possible cracks. It also helps to produce interlayer defects. Therefore, the AB 90° oriented component exhibits lower yield and tensile strengths (Figure 3.11).

For AB 0° oriented components, the axis of applied load was perpendicular to the build direction, resulting in the largest yield and tensile strengths. The tensile specimens with AB 0° build orientation showed the minimum ductility, despite similar microstructure for the differently oriented samples. Due to uneven powder distribution of successive layers, defects are generated that reduce the elongation at fracture for 0° tensile specimens. After heat treatment, the residual stresses were relieved, but 90° oriented samples still had some interlayer defects; as a result, it showed the lowest strength.

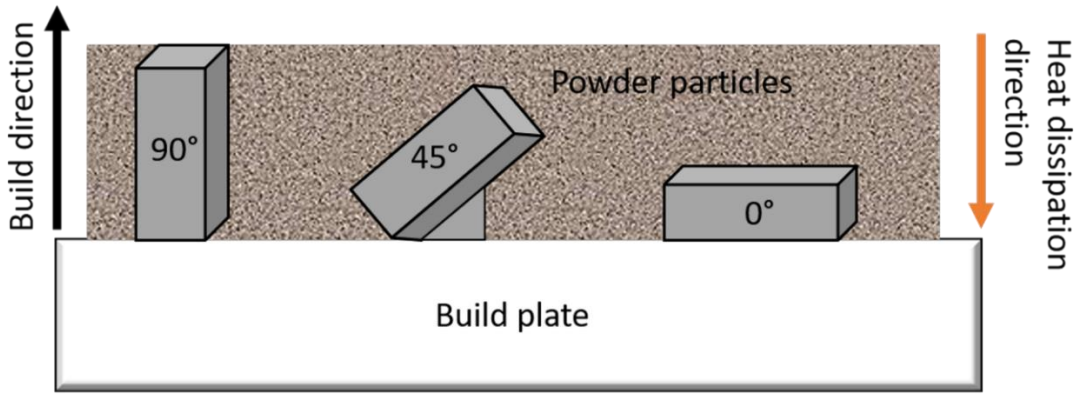

Figure 3.12 Schematic of upright, inclined and flat (edge) components with build plate

3.1.9 Fractography of as-built and heat-treated samples

Fracture analysis of the tensile tested samples was carried out to understand the correlation of fracture mechanism with microstructure of the tensile specimens fabricated in different build orientations. Surface profiles of the fractured tensile specimens are shown in Figure 3.13 and Figure 3.14, in which the fractured surfaces are generally rough and dimpled. L-PBF fabricated Ti-6Al-4V has fine α grains with weak texture and no α-colonies. Crack propagation is generally dependent on α grain orientations, consisting of multiple grain orientations in the microstructure. Because the grains have numerous crystallographic orientations (poor texture), cracks deflect at grain boundaries, resulting in intergranular fracture [14].

The build orientations influence surface roughness of core region of the fracture surface profile because the specimen fractures either along α grain boundaries that pass through entire prior-β grains or along the boundaries of prior-β grains. In 0º (flat) oriented tensile specimens, prior-β grain boundaries are perpendicular to the loading axis because the solidification was opposite to the heat dissipation and perpendicular to the loading axis during fabrication as shown in Figure 3.12. The intergranular fracture along these grain

boundaries produced a smoother surface profile. The prior-β grain boundaries in 90º oriented specimens are approximately along the loading axis. When compared to other build-oriented specimens, the fracture through grain boundaries has produced elusive crack patterns and rough fracture surface profiles as shown in Figure 3.13 and Figure 3.14. From Figure 3.13 (b) and Figure 3.14 (a) and (b), we can conclude that around the region of pores, the fractured surface is less rough and also concentric in nature; the same morphology is also reported by Hartunian and Eshraghi [11].

However, it is difficult to differentiate whether fracture surfaces had initiated from the pore region or from any other region. Terrace-like features are present mostly in HT tensile specimens in different build orientations. Terraces have a rich topography where the powder is partially melted and defects are produced as shown in the insets of Figure 3.13 (a), (b), and Figure 3.14 (a). Terraces arose as a result of lamellar fracture as shown in the inset of Figure 3.14 (b); this trend is reported by Hartunian and Eshraghi [11].

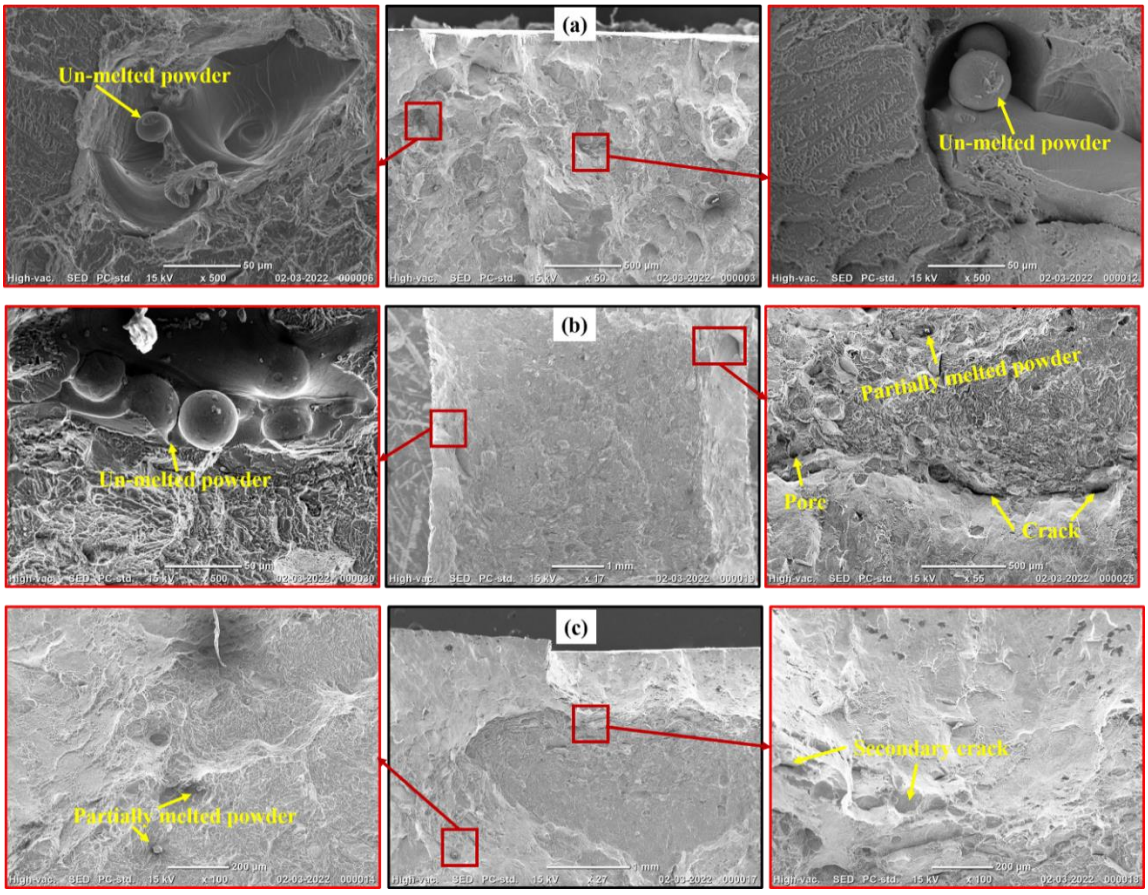

Figure 3.13 SEM micrographs of fracture surfaces of tensile test specimens illustrating the presence of defects corresponding to the (a) AB-0º, (b) AB-45º, and (c) AB-90º samples

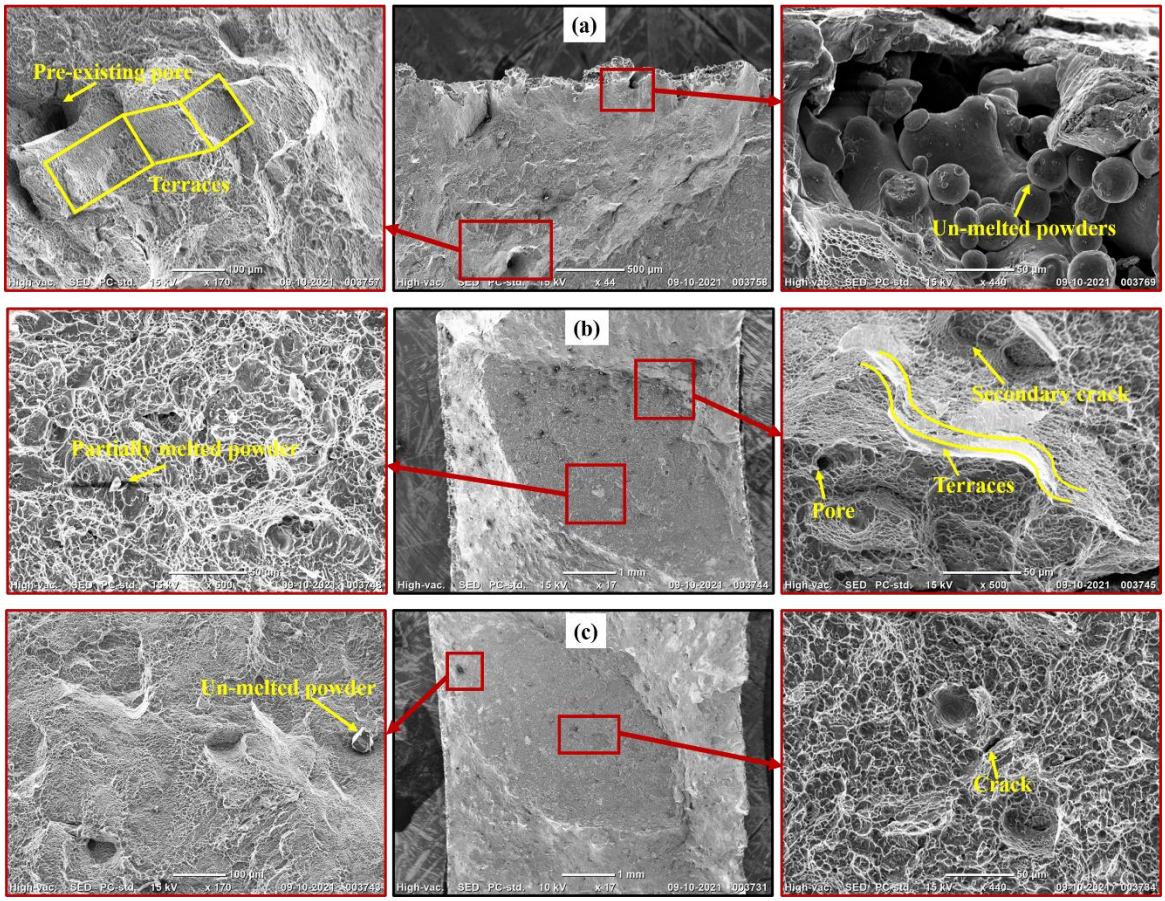

Figure 3.14 SEM micrographs of fracture surfaces of tensile test specimens illustrating the presence of defects corresponding to the (a) HT-0º, (b) HT-45º, and (c) HT-90º samples

With the above results and discussion of microstructure and mechanical properties of additively manufactured Ti-6Al-4V alloy, results and discussion of surface characteristics of AM fabricated Ti-6Al-4V alloy has been discussed in chapter 4.